# Absolute instability of moisture-coupled waves on the equatorial beta-plane

Cameron G MacDonald[1]

[1]Program in Atmospheric and Oceanic Science, Princeton University

May 25, 2023

**Abstract**

The instabilities produced by a linear model of the tropical atmosphere coupled to a prognostic equation for water vapour are investigated. For parameter regimes relevant to the Indo-Pacific warm pool, the long-time asymptotic behaviour of the unstable waves is found to be absolutely unstable, so that the amplitude of disturbances will grow in time at every point in the domain. Other limits of the system do not produce this same behaviour at these length and time scales. It is shown that the resultant long-time behaviour of the instability is characterized by roughly equal roles for temperature and moisture fluctuations in setting the thermodynamic tendency of the waves. Under the assumption of a zonally varying flow, it is shown analytically that localized regions of instability may be formed, again using parameter choices relevant to the warm pool. The dynamics and thermodynamics of these local instabilities show some correspondence with the observed development of the Madden-Julian Oscillation as it propagates through the warm pool.

*(Submitted to the Quarterly Journal of the Royal Meteorological Society)*

**ORIGINAL ARTICLE**

**Journal Section**

# Absolute instability of moisture-coupled waves on the equatorial beta-plane

**Cameron G. MacDonald**[1]

[1]Program in Atmospheric and Oceanic Science, Princeton University, Princeton, NJ, 08544, United States

**Correspondence**
C. G. MacDonald, Sayre Hall, 300 Forrestal Road, Princeton, NJ, 08540, United States
Email: cgm3@princeton.edu

**Funding information**
Cooperative Institute for Modeling the Earth System (CIMES), Princeton University/NOAA GFDL

The instabilities produced by a linear model of the tropical atmosphere coupled to a prognostic equation for water vapour are investigated. For parameter regimes relevant to the Indo-Pacific warm pool, the long-time asymptotic behaviour of the unstable waves is found to be absolutely unstable, so that the amplitude of disturbances will grow in time at every point in the domain. Other limits of the system do not produce this same behaviour at these length and time scales. It is shown that the resultant long-time behaviour of the instability is characterized by roughly equal roles for temperature and moisture fluctuations in setting the thermodynamic tendency of the waves. Under the assumption of a zonally varying flow, it is shown analytically that localized regions of instability may be formed, again using parameter choices relevant to the warm pool. The dynamics and thermodynamics of these local instabilities show some correspondence with the observed development of the Madden-Julian Oscillation as it propagates through the warm pool.

**KEYWORDS**
absolute instability, tropical dynamics, Madden-Julian Oscillation, Kelvin waves, moist thermodynamics, waves, instability

# 1 | INTRODUCTION

Significant challenges remain in the theory and modelling of tropical waves in the atmosphere (Kiladis et al., 2009; Jiang et al., 2020). It is now recognized that inclusion of a prognostic equation for atmospheric water vapour in a linear shallow water model allows for the emergence of modes whose characteristics can resemble those of observed low-frequency convectively-coupled equatorial waves and the Madden-Julian Oscillation (MJO) (Neelin and Yu, 1994; Sobel et al., 2001; Adames and Maloney, 2021). Such models rely on moist convection to reduce the effective static stability felt by disturbances in the tropics to produce phase speeds much less than the dry gravity wave speed (Emanuel et al., 1994; Kiladis et al., 2009). Additional modification of the effective stability by diabatic or advective processes is important for producing instability at planetary scales (Adames and Kim, 2016; Inoue and Back, 2017; Ahmed et al., 2021). Under such conditions, it is possible for thermodynamics to be controlled primarily by fluctuations of moisture. This has led to the definition of "moisture modes" as a particular limit of the behavior of tropical waves (Ahmed et al., 2021). In general, the tropics may support a diverse spectrum of disturbances ranging from gravity waves to moisture modes (Roundy, 2012; Adames et al., 2019).

These theories provide a relatively simple picture of the fundamental interactions between dynamics and convection that generate low-frequency tropical waves. However, previous linear stability analysis of these waves has largely been concerned with the normal modes of the system, and as such little attention has been focused to the spatial instability of these wave solutions, as opposed to their temporal instability. While some studies have explored the interaction between simple models of the MJO and a zonally asymmetric basic state (Majda and Stechmann, 2011; Raymond and Fuchs, 2018), more theoretical work is needed on this topic. Earth's zonal asymmetry limits the convective signal of the MJO primarily to the Indo-Pacific warm pool (WP), and the characteristics of the MJO change significantly as it propagates through the WP (Hendon and Salby, 1994). It was shown by Hendon and Salby (1994) that MJO initiation over the Indian Ocean is associated with planetary-scale temperature and heating anomalies that are largely in phase, leading to wave growth, while over the Central Pacific the anomalies are more in quadrature. Furthermore, the thermodynamics of the MJO are more controlled by moisture in the Indian Ocean (Adames and Kim, 2016), and become more gravity wave-like as the convecting region propagates into the Central Pacific (Sobel and Kim, 2012; Mayta and Adames, 2023). Model experiments have shown that imposition of zonal asymmetries mimicking the WP can significantly enhance MJO-like variability (Maloney et al., 2010; MacDonald and Ming, 2022). The mechanisms for the zonal development of the MJO and its moisture mode-gravity wave transition also demand more theoretical investigation. From the standpoint of linear models for the MJO, these considerations necessitate a move beyond analysis of normal modes embedded within uniform basic states.

In the study of unstable flows, an important distinction must be made between waves that are convectively unstable and those that are absolutely unstable (Briggs, 1964; Huerre and Monkewitz, 1985). As explained by Briggs (1964), absolute instabilities will grow in amplitude at every point in space, while convective instabilities will grow in an envelope around the peak of the disturbance, eventually decaying at every point in space after sufficient time has passed. This concept has been well-studied in simple analogues of mid-latitude flow (Merkine, 1977; Simmons and Hoskins, 1979; Farrell, 1982; Pierrehumbert, 1986; Lin and Pierrehumbert, 1993). Applying the theory set out by Briggs (1964), the pioneering study of Merkine (1977) showed that a two-level model on the midlatitude $\beta$-plane could support absolute instability. However, the ultimate conclusion of Lin and Pierrehumbert (1993) was that the typical midlatitude flow on Earth is not absolutely unstable in the presence of a westerly surface wind, and hence a localized storm track cannot sustain wave energy indefinitely, and instead requires disturbances to enter from upstream. The presence of absolute instability in a zonally varying flow is necessary for the development of localized regions of instability (Pierrehumbert, 1984; Huerre and Monkewitz, 1990).

Recently, these concepts have been applied to the study of African easterly waves (Diaz and Aiyyer, 2015) and monsoonal disturbances (Rupp and Haynes, 2020). Diaz and Aiyyer (2015) showed that African easterly waves can disperse energy upstream, and are thus able to seed the growth of further wave crests without an external forcing. Rupp and Haynes (2020) related different regimes of monsoonal anticyclone flows to the underlying absolute or convective nature of the instability. They further highlighted another important feature of absolutely unstable systems, namely their insensitivity to the specifics of the imposed forcing, provided the forcing is not growing in time at a rate faster than the absolute growth rate (Briggs, 1964).

In this study we will investigate the implications of absolute instability on equatorial waves when coupled to an equation for atmospheric water vapour. It will be shown that in uniform basic states representing the WP that the emergent low-frequency unstable waves are in fact absolutely unstable. In the next section, we will develop the linear equations with which we will work, and review the concepts of absolute and convective instability. Section 3 will identify the nature of the instabilities in the system, and show that local instability is supported under certain parameter regimes. A discussion of results and their connection to the observed characteristics of the MJO is provided in Section 4. Finally, concluding remarks are given in Section 5.

## 2 | THEORETICAL BACKGROUND

### 2.1 | A Linear Model for the Tropical Atmosphere

The primitive equations on the equatorial $\beta$-plane linearized about a state of rest are given in pressure coordinates by (Fulton and Schubert, 1985)

$$\frac{\partial \mathbf{v}}{\partial t} + \beta y \mathbf{k} \times \mathbf{v} + \nabla \phi = 0, \tag{1a}$$

$$\frac{\partial \phi}{\partial p} = -\frac{R_d T}{p}, \tag{1b}$$

$$\nabla \cdot \mathbf{v} + \frac{\partial \omega}{\partial p} = 0 \quad \text{and,} \tag{1c}$$

$$C_p \frac{\partial T}{\partial t} + \omega \frac{\partial \overline{s}}{\partial p} = Q. \tag{1d}$$

The stratification is set by the vertical gradient of the basic state dry static energy, $\partial \overline{s}/\partial p$, and all other notation is standard. In the absence of friction in the momentum equation, the system is closed but for the heating rate $Q$. The vertically-integrated version of Equation (1d) is given by

$$C_p \frac{\partial \langle T \rangle}{\partial t} + \left\langle \omega \frac{\partial \overline{s}}{\partial p} \right\rangle = \langle Q \rangle, \tag{2}$$

where $\langle \cdot \rangle$ represents a pressure integral from the surface to the tropopause. Rather than express $\langle Q \rangle$ in terms of the primitive variables, we introduce a prognostic equation for the column water vapour $\langle q \rangle$ of the atmosphere and write

the heating rate as a function of $\langle q \rangle$ (Neelin and Yu, 1994). The equation for $\langle q \rangle$ takes the form

$$\frac{\partial \langle q \rangle}{\partial t} = -\langle \mathbf{v} \cdot \nabla q \rangle - \left\langle \omega \frac{\partial q}{\partial p} \right\rangle + E - P, \tag{3}$$

where $E$ is the evaporation from the surface and $P$ is the precipitation from the atmosphere. The latent heat of vapourization has been absorbed into $\langle q \rangle$, $E$ and $P$ so that they have energy units. The system is greatly simplified by assuming that there is no meridional wind. While this simplification may seem severe (in the dry system it eliminates all equatorial modes but for the Kelvin wave), past studies have shown that many of the essential features of eastward-propagating intraseasonal variability can still be captured with such a model (Fuchs and Raymond, 2017; Kim and Zhang, 2021; Wang and Sobel, 2022a). The pressure velocity $\omega$ is then assumed to have separable vertical structure $\Lambda_\omega(p)$ of a first baroclinic mode, being zero at the surface and tropopause and attaining a maximum in the mid-troposphere. The primitive equations can then be used to relate the vertical structures of $u$, $\phi$ and $T$ to $\Lambda_\omega$. Such systems have been developed in a number of previous works (Fuchs and Raymond, 2017; Adames et al., 2019; Ahmed et al., 2021; Wang and Sobel, 2022a). The equations can then be written as

$$\frac{\partial u_1}{\partial t} + \frac{\partial \phi_1}{\partial x} = 0 \tag{4a}$$

$$\beta y u_1 + \frac{\partial \phi_1}{\partial y} = 0 \tag{4b}$$

$$-\frac{M_s}{c^2}\frac{\partial \phi_1}{\partial t} = M_s \frac{\partial u_1}{\partial x} + \frac{(1+r)}{\tau_c}\langle q \rangle \tag{4c}$$

$$\frac{\partial \langle q \rangle}{\partial t} = -M_q \frac{\partial u_1}{\partial x} - \frac{1}{\tau_c}\langle q \rangle - A_q u_1, \tag{4d}$$

where $(\cdot)_1$ indicates the horizontal structure of a field. Here $c = 50$ m s$^{-1}$ is the dry gravity wave speed, $M_s = \langle -\Lambda_\omega \partial_p \overline{s} \rangle$ is an integrated measure of the dry stability of the atmosphere, $M_q = \langle \Lambda_\omega \partial_p \overline{q} \rangle$ is a measure of the integrated moisture stratification, and $\tau_c$ is a convective relaxation time introduced by parametrising the precipitation as $P = \langle q \rangle / \tau_c$. The parameter $r$ is a cloud-radiative feedback parameter which relates radiative heating to precipitation, and $A_q$ represents moistening processes such as wind-evaporation feedback, eddy moisture fluxes and frictional convergence that are associated with the zonal wind (Sobel and Maloney, 2013; Adames and Kim, 2016; Adames et al., 2019). Essentially, we have collected all the terms on the right-hand side of Equation (3) but for the precipitation and vertical advection by the first baroclinic mode, and assumed that these remaining terms can be linearly related to the zonal wind.

We will now present the normal mode solutions of the form $u_1 \propto e^{i(kx-\sigma t)}$, with wavenumber $k$ and frequency $\sigma$. For a separable meridional structure, Equations (4a) and (4b) may be combined to show that all the fields in the model have the shape

$$\mathcal{P}(y) = \exp(-\beta k y^2/(2\sigma)). \tag{5}$$

It then follows that for real $k$ and $\mathrm{Re}(\sigma) > 0$, solutions with $k < 0$ will not be equatorially trapped and thus do not hold any physical relevance. Combining Equations (4a), (4c), and (4d) and eliminating $\phi_1$ and $\langle q \rangle$ gives a governing equation for the system:

$$\left(\frac{\partial}{\partial t} + \frac{1}{\tau_c}\right)\frac{\partial^2 u_1}{\partial t^2} - c^2\frac{\partial^3 u_1}{\partial x^2 \partial t} - c^2\frac{\tilde{M}_e}{\tau_c}\frac{\partial^2 u_1}{\partial x^2} + c^2\frac{\tilde{A}_q}{\tau_c}\frac{\partial u_1}{\partial x} = 0, \tag{6}$$

where $\tilde{M}_e = (1+r)(1 - M_q/M_s) + r$ is the effective gross moist stability (GMS), and $\tilde{A}_q = (1+r)A_q/M_s$ is a rescaled moistening parameter with units of inverse length (Adames et al., 2019). The corresponding dispersion relation is given by

$$\mathcal{D}(k,\sigma) = \tau_c\sigma^3 + i\sigma^2 - \tau_c c^2 k^2 \sigma - ic^2k^2(\tilde{M}_e + i\tilde{A}_q k^{-1}) = 0. \tag{7}$$

The cubic term in $\sigma$ is small relative to the quadratic term since the convective timescale $\tau_c$ is much faster than the timescale of the waves. Wang and Sobel (2022a) showed that for certain parameter choices, neglecting this term filters a Kelvin wave damped at the convective timescale. However, Adames et al. (2019) showed that for a much shorter convective timescale and positive effective GMS, Kelvin waves that are unstable at planetary scales exist under this approximation. The filtered mode becomes near stationary in this limit, remaining damped at the shortened convective timescale. It is then understood that this simplification filters out the initial adjustment process to a quasi-equilibrium (QE) state. These various limits of the system were also isolated by way of an asymptotic expansion by Ahmed et al. (2021). Since we are primarily concerned with asymptotic behaviour, the strongly damped convective adjustment is not of particular interest. The resulting dispersion relation is then

$$\mathcal{D}(k,\sigma) = i\sigma^2 - \tau_c c^2 k^2 \sigma - ic^2k^2(\tilde{M}_e + i\tilde{A}_q k^{-1}) = 0. \tag{8}$$

The forthcoming analysis will also necessitate solving the dispersion relation for $k$ as a function of given $\sigma$. $\mathcal{D}(k,\sigma)$ may be written in powers of $k$ as

$$\mathcal{D}(k,\sigma) = -c^2(\tau_c\sigma + i\tilde{M}_e)k^2 + c^2\tilde{A}_q k + i\sigma^2 = 0. \tag{9}$$

Solutions for $\sigma(k)$ produce one root that is unstable at planetary scales. The other root produces negative $\sigma_r$ for all real $k$, and thus does not satisfy boundary conditions at infinity. In general, both roots of $k(\sigma)$ hold physical relevance.

Figure 1a shows the frequency of the unstable solution in three separate parameter regimes. For large values of $\tau_c$ and small or negative values of $\tilde{M}_e$ the solution takes on the character of a QE mode (Ahmed et al., 2021; Wang and Sobel, 2022a), while for small values of $\tau_c$ and large $\tilde{M}_e$ it behaves like a Kelvin wave. Specifically, we set $\tilde{M}_e = 0$ and $\tau_c = 12$ h to achieve the QE regime, and use $\tilde{M}_e = 0.2$ and $\tau_c = 2$ h for the Kelvin regime. In all cases the moistening process has been set to $\tilde{A}_q = 2\times10^{-8}$ m$^{-1}$ (Adames et al., 2019). In the limit where the gravity wave speed is made infinite, the solutions become moisture modes, with thermodynamics controlled by moisture perturbations (Ahmed et al., 2021). The Kelvin wave is essentially non-dispersive, while the frequency of the moisture mode has a $k^{-1}$ dependency; the QE mode is in some sense a smooth transition between these two regimes. Interestingly, this transition causes the QE regime to have a lower frequency at $k = 1$ than either of its limiting cases. The corresponding growth rates are shown in Figure 1b. Both the Kelvin wave and QE mode are unstable at planetary scales, while the growth rate of the moisture modes takes on a constant value of $-\tilde{M}_e/\tau_c$. The phase speeds of the waves are shown in Figure 1c. The horizontal structures of the planetary scale waves in each regime are shown in Figure 1d-f. For

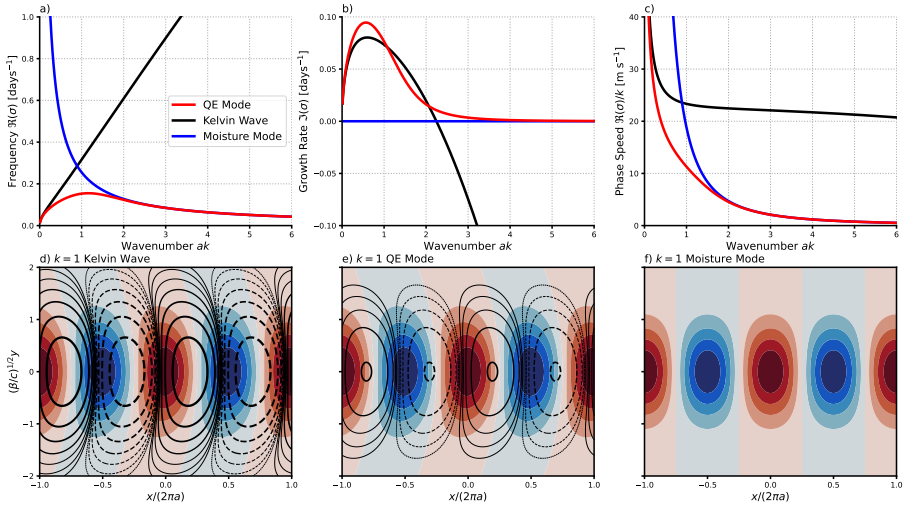


**FIGURE 1** (a) Frequency $\sigma_r(k)$ of the unstable mode in the three different regimes for the system. (b) Growth rate $\sigma_i(k)$ of the unstable mode. (c) Phase speed $\sigma_r/k$ of the unstable mode. (d) spatial structure of the $k = 1$ Kelvin mode for a unit perturbation of column water vapour $\langle q \rangle$ (shading). The contours show the corresponding column temperature perturbations $-M_s\phi_1/c^2$. The contours are in powers of 2, with the thinnest contours at $\pm 1/8$ and the thickest at $\pm 8$. (e) As in (d) but for the QE regime. (f) As in (d) but for the moisture mode regime, in which temperature perturbations are negligible.

the Kelvin and QE modes, moisture and temperature are slightly in phase, indicating growth of variance since the convective heating is proportional to moisture. The column temperature perturbations of the Kelvin wave are roughly an order of magnitude larger than the moisture perturbations, while for the QE mode the two fields are of the same order. For the moisture mode the temperature perturbations are negligibly small relative to moisture, and instability requires a negative effective GMS so that the overturning circulation imports more moist static energy than it exports.

## 2.2 | Numerical Methods

Some numerical simulations will be performed to motivate the theoretical results derived from the dispersion relation. In these numerical simulations we allow the parameters of the model $\tilde{M}_e$, $\tau_c$, and $\tilde{A}_q$ to be spatially varying, so that the system can be written in matrix form as

$$\frac{\partial}{\partial t}\begin{pmatrix} u_1 \\ \dot{u}_1 \end{pmatrix} = \begin{pmatrix} 0 & 1 \\ c^2\partial_x(\tilde{M}_e\partial_x\cdot) - c^2\partial_x(\tilde{A}_q\cdot) & c^2\partial_x(\tau_c\partial_x\cdot) \end{pmatrix}\begin{pmatrix} u_1 \\ \dot{u}_1 \end{pmatrix} + \begin{pmatrix} 0 \\ F \end{pmatrix}, \tag{10}$$

where $\dot{u}_1 = \partial_t u_1$ and $F$ is a forcing term which excites the system from an initial state of rest. The zonal coordinate is non-dimensionalized as $x = 2\pi a\hat{x}$, and time as $t = (\beta c)^{-1/2}\hat{t}$, where $a$ is the radius of Earth. The shape of the forcing is given by

$$F(x,t) = \begin{cases} F_0\cos^2(\pi\hat{x})\delta(\hat{t}) & \text{if } |\hat{x}| < 1/2 \\ 0 & \text{otherwise,} \end{cases} \tag{11}$$

where $F_0$ is the amplitude of the forcing and $\delta(\cdot)$ is the Dirac delta function. The spatial coordinate, which ranges from $\hat{x} = -20$ to $\hat{x} = 20$, is decomposed into 512 Fourier components. Terms that are the product of two spatially varying quantities are evaluated using the spectral transform method (Durran, 2013). The system is stepped forward in time using a 3rd order Adams-Bashforth scheme, with two initial 4th order Runge-Kutta steps to initialize the time-stepping procedure. An additional $\partial_x^4$ diffusion term has been added to the system to remove energy at the smallest scales, but does not appreciably affect the behaviour at the scales of interest.

## 2.3 | Absolute and Convective Instability

We now review some essential points about the concepts of absolute and convective instability. It is evident from the dispersion diagrams shown in Figure 1 that outside the moisture mode limit, there exists some wavenumber at which $d\sigma_i/dk = 0$, where $\sigma_i = \Im(\sigma)$ is the imaginary part of the frequency. That is, the system has a most unstable wavenumber $k_m$. Consider now the evolution of the system in time from an arbitrary initial condition

$$u_1(x,t) = \int_{-\infty}^{\infty} \mathcal{U}(k) e^{i(kx-\sigma(k)t)}\, dk, \tag{12}$$

where $\mathcal{U}(k)$ sets the initial shape of the pulse. In the asymptotic limit as $t \to \infty$, the behaviour of the integral in Equation (12) is dominated by its point of stationary phase, which for a given $x$ and $t$ is the wavenumber $k_s$ that satisfies $x/t = d\sigma/dk|_{k_s}$. Taking a second-order Taylor expansion of $\sigma(k)$ about $k_s$ yields the expression

$$u_1(x,t) \sim \frac{\sqrt{2\pi} e^{-i\pi/4} \mathcal{U}(k_s)}{\left((d^2\sigma/dk^2)|_{k_s} t\right)^{1/2}} e^{i(k_s x - \sigma(k_s)t)} \quad (t \to \infty). \tag{13}$$

Equivalent expressions have been presented in previous work on the asymptotic behaviour of unstable waves (Gaster, 1968; Merkine and Shafranek, 1980; Pierrehumbert, 1984). A similar formulation of the asymptotic solution exists based on an arbitrary external forcing and the Green's function of the system (Briggs, 1964; Merkine, 1977). If we evaluate the above expression at the most unstable wavenumber, we must have $d\sigma_r/dk|_{k_m} = x/t$, where $\sigma_r = \Re(\sigma)$. The maximum growth rate is then associated with a characteristic that moves at the group velocity evaluated at $k_m$, i.e. the peak of the wavepacket moves at this group velocity. In general the value of maximum $\sigma_i$ for real $k$ does not provide information about the behavior at a fixed point in space. The wavenumber and frequency which dominate the asymptotic response at fixed $x = 0$ must be a saddle point of $\sigma(k)$ satisfying $d\sigma/dk = 0$, or equivalently a merge between two branches of $k(\sigma)$. Since the peak is advected with the group velocity of the most unstable wavenumber, the behaviour at a fixed point will be that of a spatially amplifying wave, and $k_s$ will in general move out into the complex plane. If $\sigma_i(k_s) > 0$ at the saddle point, then the disturbance will grow at every point in the domain, in which case the instability is called absolute. Conversely if $\sigma_i(k_s) < 0$ the instability is convective; the amplitude will eventually decay to zero for all $x$ after the peak has passed (Briggs, 1964; Huerre and Monkewitz, 1985). Figure 2 shows how these two different kinds of spatial instability would influence the growth of a localized disturbance.

In a zonally varying flow the presence of absolute instability permits, under certain conditions, the development of local instabilities (Pierrehumbert, 1984). For a uniform domain, the growth rate at the most unstable real wavenumber provides an upper bound for the absolute growth rate (Huerre and Monkewitz, 1990). Simply put, the tail of a wavepacket naturally cannot have a larger amplitude than the peak. However, if zonal variations exist such that the peak can travel into a region with sufficiently reduced instability, then the absolute growth rate of the exponential tail may exceed the now reduced growth rate of the peak, and a localized maximum of the amplitude can occur (Pierre-

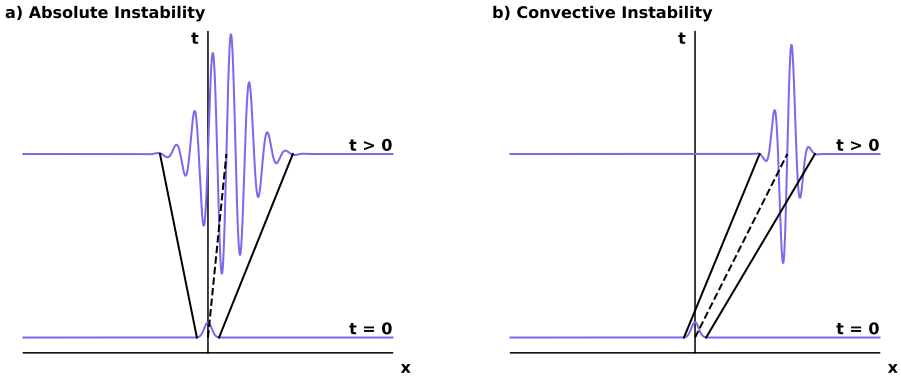


**FIGURE 2** (a) Sketch of an absolutely unstable wave packet. Starting from a localized pulse disturbance at $t = 0$, the amplitude of the wave packet disperses in both directions. Any fixed point in space will have the amplitude of the wave packet grow in time. (b) Sketch of a convectively unstable wave packet. There are some set of characteristics along which the amplitude grows in time, but for any fixed point in space the peak will eventually pass and the amplitude will decay. Based on a similar figure in Huerre and Monkewitz (1985).

humbert, 1984). Necessary conditions for the existence of a local mode are closely linked to the presence of absolute instability in a system. In the absence of local instability, a periodic domain is required to create a global instability of the system (Pierrehumbert, 1984; Huerre and Monkewitz, 1990).

## 3 | INSTABILITY OF MOISTURE-COUPLED WAVES

### 3.1 | Presence of Absolute Instability

We will first identify the nature of the instabilities in the moist equatorial wave system by analyzing the dispersion relation in the complex $k$-plane (Briggs, 1964; Merkine, 1977; Pierrehumbert, 1986). We evaluate $k(\sigma)$ for some set of fixed values of $\sigma_r$, while decreasing $\sigma_i$ from a positive value (which must be greater than the maximum growth rate for real $k$) to zero Briggs (1964). The information provided in the dispersion diagrams shown in Figure 1 is recovered when the images cross the positive real line. If the images of two branches of $k(\sigma)$ meet in the complex $k$-plane, with the branches originating separately from the upper and lower half-planes for large $\sigma_i$, then the system supports absolute instability (Briggs, 1964; Pierrehumbert, 1986). Otherwise, the branches merge for some negative value of $\sigma_i$, and the instability is convective in nature. Since the dispersion relation for our system is quadratic in $k$, there can be only one saddle point.

Figure 3 shows contours of $\sigma$ and their corresponding images for the three previously presented parameter regimes. The contours in the complex $\sigma$-plane are shown in Figure 3a. The image for the Kelvin wave is shown in Figure 3b. It is clear that there is an absolute instability present, as the two branches merge close to the imaginary line. Since this merge happens at far greater length scales than are realizable on Earth, and is only weakly unstable, it does not appear to have much physical relevance. Figure 3c shows the image for the QE regime; clearly there exists a more compelling merge of the two branches. The branches of $k$ originate separately from the upper and lower half-planes for large $\sigma_i$, confirming their physical relevance (Briggs, 1964; Pierrehumbert, 1986). The merge occurs at real wavenumber $ak_r \approx 0.75$ and linear frequency $\sigma_r/(2\pi) \approx 0.021$ days$^{-1}$ so the absolute instability is realized at

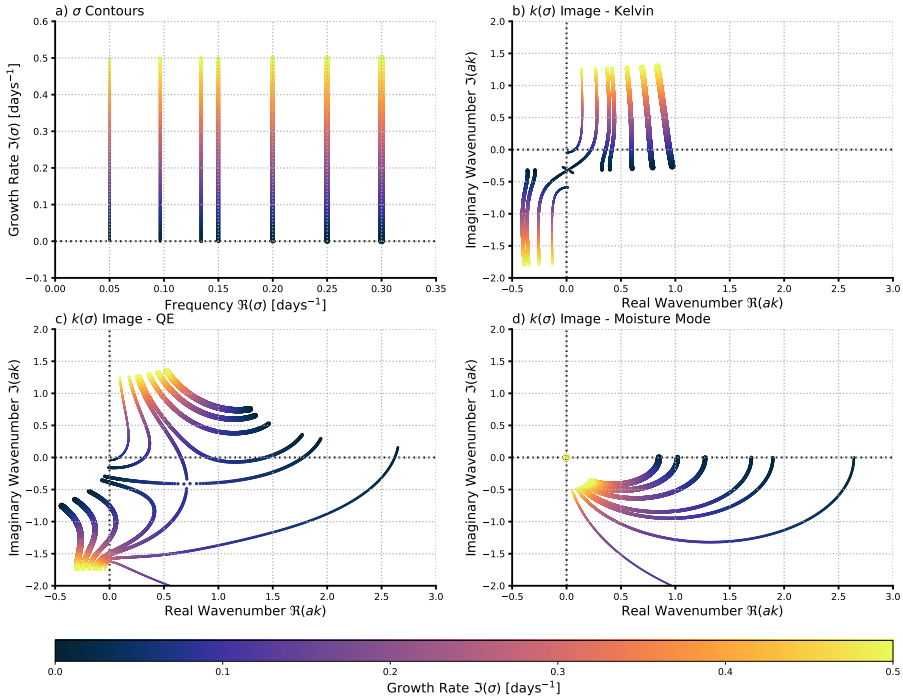


**FIGURE 3** (a) Contours in the complex $\sigma$-plane. The shading indicates the imaginary part and the thickness of the line scales with the real part of $\sigma$. (b) the image $k(\sigma)$ in the complex $k$-plane for the Kelvin parameter regime. The mapping can be tracked by the colour and thickness of the lines. (c) As in (b) but for the QE regime. A clear merge between the two branches of $k(\sigma)$ is observed in the lower half-plane. (d) As in (b) but for the moisture mode regime, in which only a single non-trivial branch exists.

planetary scales and intraseasonal frequencies. The image for the moisture mode limit is shown in Figure 3d; since there is only one non-trivial branch, there is no possibility of a merge. However, it is clear that the lower branch of the QE regime takes on some characteristics of the moisture mode.

Given that we have separated out the meridional structure of the system, we must be circumspect that these solutions remain equatorially trapped when $k$ as well as $\sigma$ is complex. For the case of complex $k$, the meridional structure can be expressed in terms of the phase speed $c_p = \sigma/k$ as

$$\mathcal{P}(y) = \exp\left(-\frac{\beta c_{p,r} y^2}{2|c_p|^2}\right) \exp\left(i\frac{\beta c_{p,i} y^2}{2|c_p|^2}\right), \tag{14}$$

where $c_{p,r} = \Re(c_p)$ and $c_{p,i} = \Im(c_p)$. The argument of the first exponential is purely real, while the argument of the second is purely imaginary. It is clear that the condition for equatorial trapping is $c_{p,r} > 0$. Figure 4 shows the real part of the phase speed evaluated on the contours in the $k$-plane presented above. The absolute instability of the QE mode is equatorially trapped. In the Kelvin wave regime, the value of $c_{p,r}$ at the absolute instability is close to zero, calling in to question the relevance of this absolute instability.

Numerical integrations of the responses of the QE and Kelvin regimes are shown in Figures 5a and 5b, respectively. It is clear that the QE wave packet grows in both directions, confirming the presence of absolute instability. The

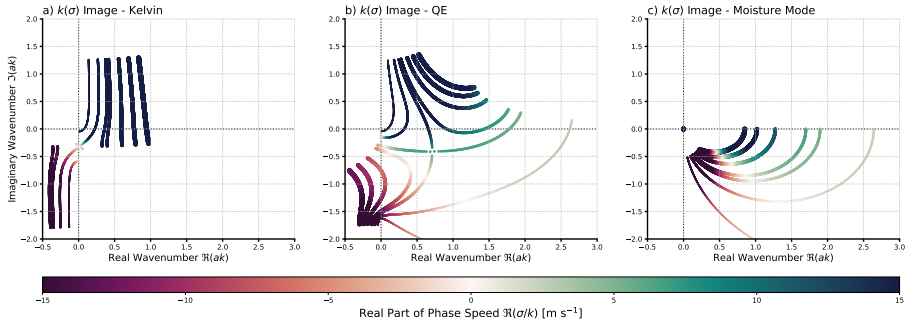


**FIGURE 4** (a) Image of $k(\sigma)$ for the Kelvin regime coloured by real part of $\sigma/k$. The $\sigma$ contours are the same as those used in Figure 3. Red colours indicate solutions which are not equatorially trapped and diverge as $y \to \infty$, while green colours correspond to valid equatorially trapped waves. (b) As in (a) but for the QE regime. (c) as in (a) but for the moisture mode regime.

Kelvin wave packet remains attached to $x = 0$, but does not show any significant growth there, alluding to its marginal absolute instability; that the wavelength of the Kelvin wave packet grows towards $x = 0$ is also consistent with the theoretical prediction from the analysis of the dispersion relation, where the absolute instability occurs at a much smaller wavenumber than the most unstable real wavenumber.

Figure 6 shows the amplitude growth over time, for both the translating peak of the disturbance and the stationary point $x = 0$. Figure 6a shows these growth rates for the QE regime. It is clear that the theoretical predictions of the maximum growth rate and the absolute growth rate correctly characterize the amplitude of the peak and $x = 0$, respectively. Figure 6b shows the corresponding peak and absolute growth rates for the Kelvin regime of the system. Here the marginal absolute instability is clear; the amplitude at $x = 0$ shows a negligible tendency towards growth, as predicted from analysis of the dispersion relation. Additionally, the peak growth rate for the Kelvin wave is slightly less than that of the QE mode, as predicted from the dispersion diagrams shown in Figure 1b

## 3.2 | Thermodynamics of Asymptotic Solutions

We are additionally interested in the degree to which the tendency of column-integrated moist enthalpy is set by perturbations to either temperature or moisture. In this simple linear system, the column-integrated moist enthalpy is given by

$$\langle h \rangle = -\frac{M_s}{c^2}\phi_1 + \langle q \rangle. \tag{15}$$

Following Ahmed et al. (2021), we use the ratio of moisture and temperature perturbations to understand which component controls the value of the moist enthalpy in each regime. For our linear model the ratio is

$$\gamma \equiv -\frac{c^2\langle q \rangle}{M_s\phi_1} = -i\frac{\tau_c\sigma(1 + c^2k^2/\sigma^2)}{1 + r}. \tag{16}$$

We know that $\tau_c\sigma \ll 1$, so the wave must be slow relative to the gravity wave frequency $ck$ in order for the moisture signal to dominate. Since $\gamma$ will be complex in general, its modulus $|\gamma|$ will be used to measure the relative magnitude of moisture and temperature perturbations, while its argument $\mathrm{Arg}(\gamma)$ describes the degree to which moisture and

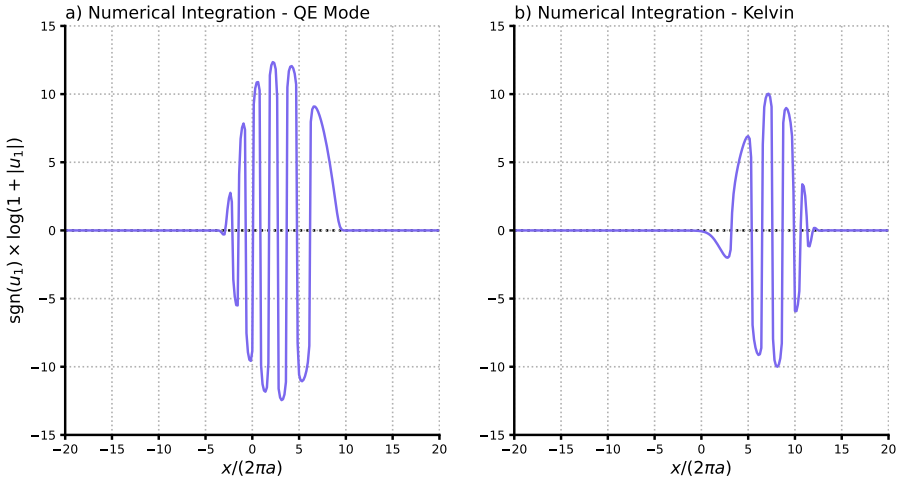


**FIGURE 5** (a) Result of a long numerical integration ($\hat{t} = 500$) of the system in the QE regime, with $\tilde{M}_e = 0$ and $\tau_c = 12$ h. The solution is transformed as $\text{sgn}(u_1)\log(1 + |u_1|)$ to better show the behaviour near the tails of the wave packet, while still retaining the fluctuations in the phase. (b) As in (a) but for the Kelvin wave parameter regime of the system, with $\tilde{M}_e = 0.2$ and $\tau_c = 2$ h.

temperature perturbations are in phase. As noted previously, this also measures the phase between temperature and heating anomalies since $\langle Q \rangle = (1 + r)\langle q \rangle / \tau_c$.

In Figure 7 we show $|\gamma|$ and $\text{Arg}(\gamma)$ evaluated on the images from the previous section. Figures 7a-c show $|\gamma|$ for each of the three parameter regimes. In the Kelvin limit temperature anomalies dominate the moist enthalpy; over the whole range of frequencies we have $|\gamma| \ll 1$. In the QE regime, solutions transition from being more gravity wave-like at large scales ($k \ll 1$) to more moisture dominated at smaller scales ($k > 1$). At the saddle point itself, temperature and moisture contribute equally to the moist enthalpy. Finally, in the moisture mode limit of the problem $|\gamma| \gg 1$ and the thermodynamics are strongly controlled by moisture.

Figures 7d-f show the same images coloured by $\text{Arg}(\gamma)$. Along the real line, all three regimes exhibit temperature and moisture anomalies that are roughly in quadrature, with temperature leading the moisture (and therefore the heating) as expected for a propagating deep-convective mode (Emanuel et al., 1994). Indeed, $\text{Arg}(\gamma)$ appears less dependent on the chosen parameter regime and more on the location in the $k$-plane. Waves that amplify in an eastward direction (those in the lower half-plane) generally have more in-phase perturbations, while those that are evanescent eastward have more out of phase relations between moisture and temperature. This is a simple consequence of the fact that an amplifying wave must have a source of variance generation; in this case the correlation between $Q$ and $T$ acts as that source. The essential convection-circulation interaction we have modeled puts a constraint on the governing thermodynamics of the system such that amplifying waves are more controlled by moisture, while evanescent waves are controlled by temperature.

## 3.3 | Zonally-Varying Basic States

Having confirmed the existence of absolute instability, we now investigate whether the system can support local modes of instability in a zonally varying flow. The Wentzel-Kramers-Brillouin (WKB) approximation will be used as a

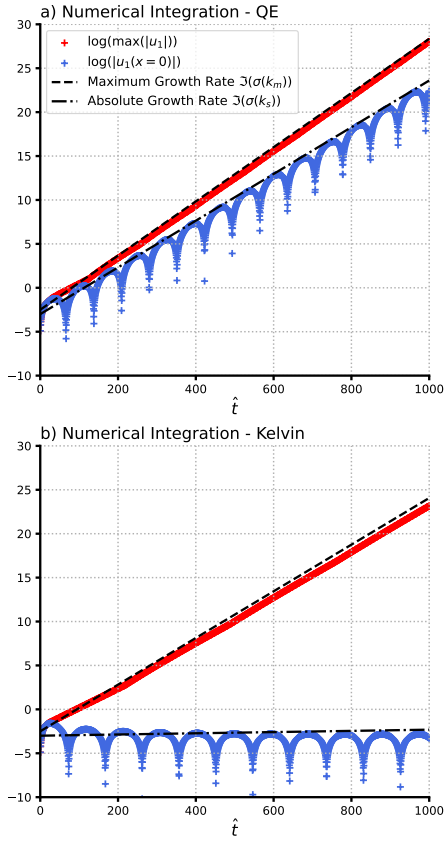


**FIGURE 6** (a) Time series of amplitude growth in the QE regime. The red crosses show the evolution of the logarithm of the maximum of $|u_1|$ achieved in the domain. The blue crosses show the value of the logarithm of $|u_1|$ at x = 0. The black dashed line shows the theoretical prediction of the maximum growth rate, $\sigma_i(k_m)/\sqrt{\beta c}$, in the non-dimensional units of the numerical simulation. The black dash-dotted line shows the predicted absolute growth rate $\sigma_i(k_s)/\sqrt{\beta c}$. (b) as in (a) but for the Kelvin wave parameter regime of the system.

theoretical tool to investigate this issue. Direct association with the observed MJO is then challenging, because the MJO can be broadly thought of as a wavenumber 1 disturbance situated in a basic state that varies most strongly at similar length scales. Strict application of the following theory is limited to infinite domains with basic state variations occurring over much longer length scales than the wavelength of the disturbance. Nevertheless, recent work has shown that local application of linear wave criteria can provide qualitative understanding of the zonal development and confinement of the MJO and other modes of tropical variability (Inoue et al., 2021; Mayta and Adames, 2023).

The construction of the local mode follows closely that of Pierrehumbert (1984). We allow the parameters $\tilde{M}_e$ and $\tau_c$ to vary in the zonal direction at $O(1)$ in a slow coordinate $X = \epsilon x$, with $\epsilon \ll 1$. Note that no specific value is assigned to $\epsilon$; it is tacitly assumed that there is some slow scale on which the WKB approximation will hold. The eigenfunctions of the systems are then taken to have the form

$$u_1 = \mathcal{A}_u(X)e^{i\Theta(X)/\epsilon}e^{-i\sigma t}, \tag{17}$$

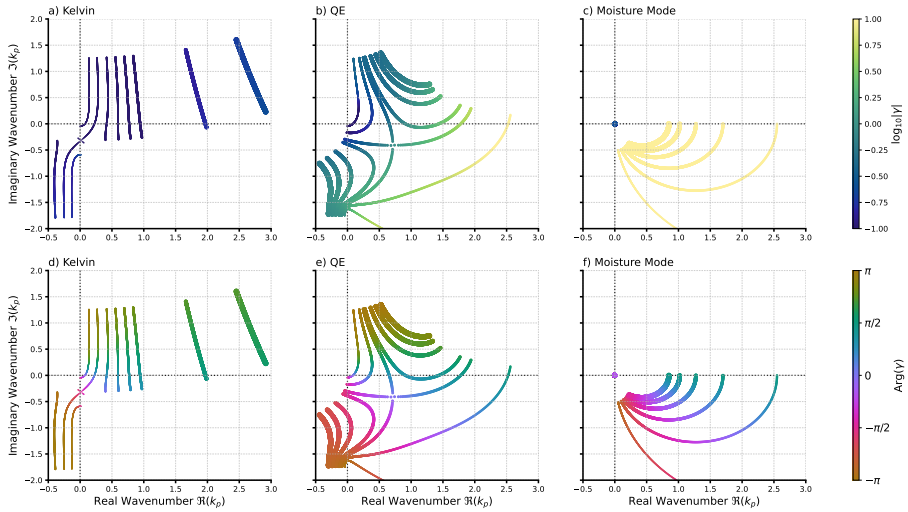


**FIGURE 7** (a) Image of $k(\sigma)$ for the Kelvin regime, coloured by $|\gamma|$. Note the log scale for the colourbar. The $\sigma$ contours are the same as those used in Figure 3. (b) As in (a), but for the QE mode. (c) as in (a), but for the moisture mode regime. (d) Image for the Kelvin regime coloured by Arg($\gamma$). A positive argument represents temperature anomalies leading moisture anomalies (to the east). (e) As in (d), but for the QE mode. (f) As in (d), but for the moisture mode limit.

where $\Theta(X)$ set the spatial amplification and phase of the wave. After suitably adjusting Equation (6) to account for varying $\tilde{M}_e$ and $\tau_c$, the dispersion relation for the system becomes, to leading order in the small parameter $\epsilon$,

$$\mathcal{D}(k,\sigma) = i\sigma^2 - c^2\Theta'^2\tau_c\sigma - ic^2\Theta'^2(\tilde{M}_e + i\tilde{A}_q\Theta'^{-1}) = 0, \tag{18}$$

where $\Theta'$, $\tilde{M}_e$ and $\tau_c$ are all functions of the slow coordinate $X$. This is simply the dispersion relation of the uniform system with the wavenumber $k$ replaced by $\Theta'(X)$. An analysis of the meridional structure problem produces an expression for the slowly varying meridional shape of the solution that bears a similar resemblance to its counterpart in the uniform system.

We now turn to the creation of a zonally varying domain that will permit a local mode of instability. Values of the parameters $\tilde{M}_e$ and $\tau_c$ are selected which produce an absolute instability with frequency $\sigma_s$; it is assumed that the system takes on these values at $X = 0$. We then calculate $k(\sigma_s; \tilde{M}_e(X), \tau_c(X))$, where $k$ has now been conflated with $\Theta'(X)$ in Equation (18). The parameters must be chosen to vary in $X$ in such a manner that the absolute growth rate—which may be calculated locally from the WKB dispersion relation for each $X$— decreases away from $X = 0$. In general, making $\tilde{M}_e$ more positive and $\tau_c$ smaller will lead to a reduction of the absolute growth rate. Requiring that the absolute growth rate attains a local maximum where $(d\tilde{M}_e/dX) = 0$ and $(d\tau_c/dX) = 0$ is important to prevent the breakdown of WKB theory (Pierrehumbert, 1984). By construction the value of $k(\sigma_s; \tilde{M}_e(0), \tau_c(0))$ is the same for the two branches of $k$, so the solution will switch branches at this point. Should the sign of $k_i(\sigma_s; \tilde{M}_e(X), \tau_c(X))$ change for one of the branches of $k$ as $X$ is moved away from zero, then the solution switches the direction in which it grows, and the constructed mode is a seamless continuation of amplifying and evanescent waves. The resulting instability is then localized in space.

Figure 8 shows how the real and imaginary parts of the wavenumber change as the basic state parameters are

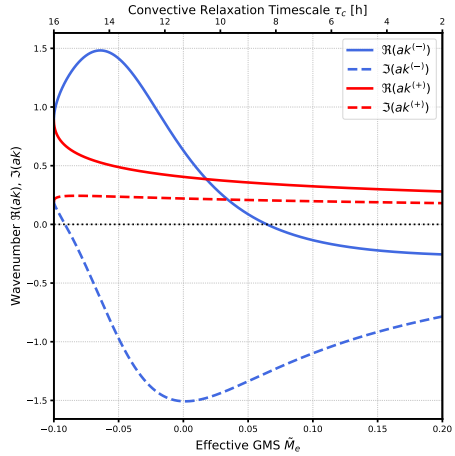


**FIGURE 8** Analysis of the WKB dispersion relation for varying basic state parameters. The parameters $\tilde{M}_e$ and $\tau_c$ are moved in proportion from values in the QE regime to the Kelvin regime. The dispersion relation is solved for $k$ as a function of $\tilde{M}_e$ and $\tau_c$, with $\sigma$ fixed to the absolute frequency calculated for $\tilde{M}_e = -0.1$ and $\tau_c = 16$ h (the values the system is assumed to take on at $x = 0$). The resulting curves for the real and imaginary parts of the wavenumber are shown in solid and dashed curves, respectively. By construction the two branches of $k$ take on the same value when $\tilde{M}_e = -0.1$ and $\tau_c = 16$ h. Note that there are some points where the two imaginary parts take on different signs.

moved together from the QE regime to the Kelvin limit. As intended, the two branches of $k(\sigma_s)$ merge at the assumed values of $\tilde{M}_e$ and $\tau_c$ which produce the largest absolute growth rate. It is clear that the imaginary parts of the two branches take on different signs when the system has been moved sufficiently far from the point of maximum absolute growth rate. The solution is able to smoothly switch between amplifying and evanescent waves and hence local modes of instability can be realized in the system. It is important to note that the system does not need to be moved far towards the Kelvin regime to produce a local mode. Sensitivity experiments with different choices of $\tilde{M}_e$ and $\tau_c$ at $x = 0$ suggest that the minimum value of $\tilde{M}_e$ in the domain must be less than zero in order for local instability to exist.

Having confirmed the potential for local instability in the system, we now look at the zonal structure of such a mode. Figure 9 shows the behaviour for a simple zonally-varying domain in which $\tilde{M}_e$ and $\tau_c$ both take on Gaussian profiles in the zonal direction (Figures 9a and 9b). Even though the branch switch itself occurs at $x = 0$, since the imaginary part of the wavenumber is positive at the coalescence point, the wave will be evanescent at $x = 0$, and will achieve its maximum amplitude at some $x < 0$. As in Section 3.2 we will use the $q$-$T$ ration $\gamma$ to characterize the thermodynamic structure of the solutions. The response of the modulus and argument of $\gamma$ as a function of $x$ are shown in Figures 9c and 9d, respectively. For $x < 0$ the thermodynamics of the mode are more controlled by moisture, and the temperature and moisture anomalies of the mode are close to being in phase. As one moves eastward through the domain, temperature and moisture perturbations transition to being more out of phase, and the thermodynamics become progressively more controlled by temperature. The importance of this asymmetric response should not be understated; a more naive local analysis of the dispersion relation for real $k$ in a zonally varying domain would not be able to describe this development. The concepts of absolute instability and branch switching play essential roles in producing the very different responses on either side of the region of increased absolute growth rate.

The theoretical predictions derived above can be checked via numerical simulation. Using Figure 8 as a guide, we

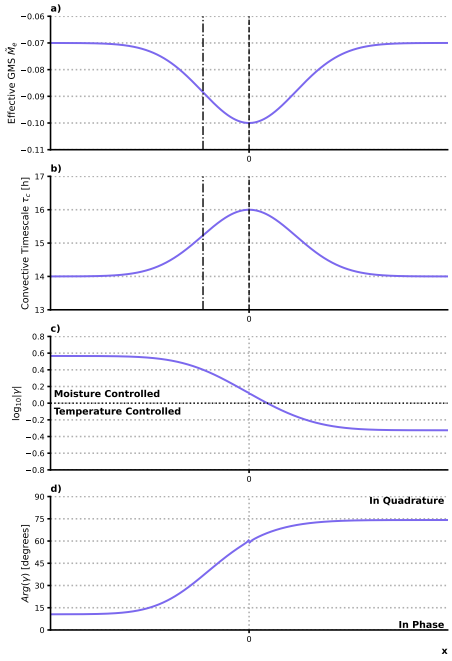


**FIGURE 9** Development of the local mode for a simple zonally-varying basic state. (a) Zonal structure of the effective GMS $\tilde{M}_e$. The chosen scale for $x$ is arbitrary. The black dashed line denotes the location at which the branch switch occurs ($x = 0$). The black dash-dotted line shows the point at which the solution switches from amplifying to evanescent. (b) As in (a), but for the convective timescale $\tau_c$. (c) Modulus of the resultant $q$-$T$ ratio $\gamma$ as a function of $x$ as predicted by the local WKB analysis. (d) Argument of $\gamma$ as a function of $x$ for the local mode.

construct a zonally varying domain where $\tilde{M}_e$ and $\tau_c$ have the structures

$$\tilde{M}_e = -0.07 - 0.03\exp(-\hat{x}^2/(2L_w^2)) \quad \text{and} \tag{19a}$$

$$\tau_c = 14 + 2\exp(-\hat{x}^2/(2L_w^2)), \tag{19b}$$

where $\tilde{M}_e$ is dimensionless and $\tau_c$ is given in units of hours, and $L_w$ is a length scale that controls the width of the region of increased instability. Thus the profiles of $\tilde{M}_e$ and $\tau_c$ resemble those shown in Figures 9a and 9b, with $L_w$ setting the zonal scale. The specific values of the parameters are chosen such that the imaginary parts of the two branches of $k(\sigma_s)$ take on different signs as $x \to \infty$. Moving the system too far into the Kelvin regime when moving away from $x = 0$ can lead to solutions that are not equatorially trapped. Figure 10 shows snapshots of $\langle q \rangle$ and $\langle T \rangle$ in two different domains: one with $L_w$ large relative to the wavelength of the local mode, and one where $L_w$ is on the same order as the wavelength. Moving eastward through the domain, temperature becomes progressively larger in magnitude relative to moisture, and the fields transition from being essentially in phase to in quadrature within the interval $[-5, 5]$. Thus the two qualitative predictions of the WKB analysis hold true in the numerical simulations. Indeed, even when the variation in the basic state is confined to a relatively short region (Figure 10b), these same zonal

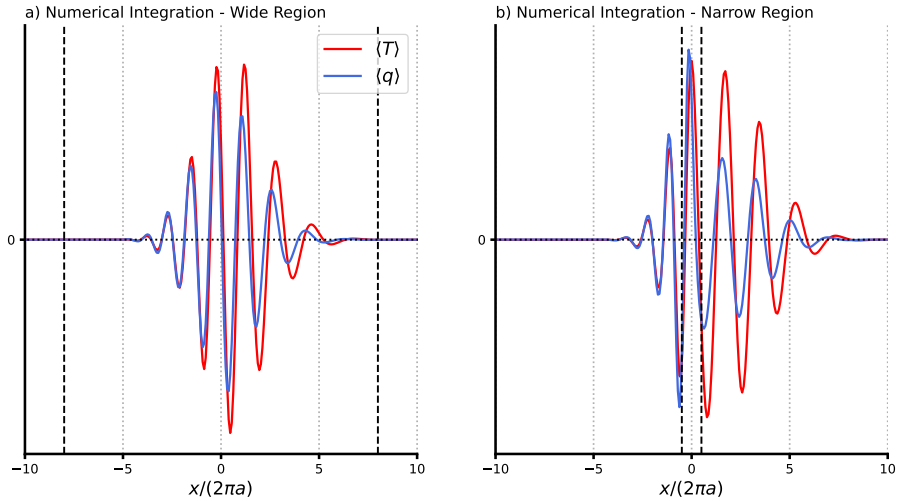


**FIGURE 10** (a) Snapshot of the numerical simulation at $\hat{t} = 1000$ for a zonally-varying basic state with $L_w = 4$. The column-integrated temperature perturbation $\langle T \rangle = -M_s \phi_1 / c^2$ is shown in red, and the column-integrated water vapour $\langle q \rangle$ in blue. The vertical dashed lines are located at $\pm 2L_w$. (b) As in (a) but for a simulation with a much narrower region of zonal variations, with $L_w = 0.25$.

variations are observed in the system. The primary alteration when using a narrow region of increased instability is that the envelope of the wave becomes more asymmetric about $x = 0$, in particular for the column water vapour $\langle q \rangle$ (Figure 10b).

Another important assumption built into the WKB analysis of the local mode is that every point in the domain grows with the absolute growth rate evaluated at $x = 0$. Figure 11 shows the evolution of the amplitude at three different locations in the domain. It is clear that after an initial adjustment period, all three locations take on essentially the same exponential growth rate, which matches well with the predicted absolute growth rate evaluated at $x = 0$. It is important to note that we have not enforced the local mode dynamics in these numerical experiments; in simply stepping the system forward in time we observe behaviour that greatly resembles the predictions made by the theory of absolute instability.

## 4 | DISCUSSION

### 4.1 | Implications for Intraseasonal Variability

The analysis presented above has shown that the response of a simple model of low-frequency moisture-coupled waves responds asymmetrically across a symmetric region of increased instability. The observed development matched the theoretical predictions provided by a WKB analysis of the system, guided by the underlying knowledge that the relevant solutions are in fact absolutely unstable. In our idealized domain, the asymmetry is such that heating and temperature perturbations are more in phase for $x < 0$ and more in quadrature for $x > 0$. Together with these phase variations, the column-integrated moist enthalpy transitions from being controlled more by moisture perturbations for $x < 0$ to temperature perturbations for $x > 0$. The resulting zonal structure of the local instability is compelling because it replicates some of the features of the zonal development of the MJO. In particular, the transition of the

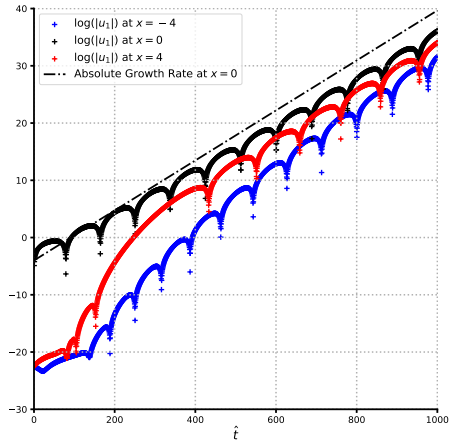


**FIGURE 11** Amplitude growth in time at three different points in the zonally varying simulation with a wide region of increased instability. The crosses denote the logarithm of $|u_1|$ at $x = -4$ (blue), $x = 0$ (black), and $x = 4$ (red). The dash-dotted line shows the predicted absolute growth rate at $x = 0$.

phase between moisture (and therefore heating) and temperature is reminiscent of the transition seen in the observed MJO (Hendon and Salby, 1994). The gradual transition of the relative magnitudes of moisture and temperature perturbations also mimics the development of the MJO (Mayta and Adames, 2023).

Absolute instability has important implications for the initiation of the MJO, in particular for "successive" MJO events which are directly preceded by a previous cycle of the oscillation (Matthews, 2008). Powell and Houze Jr (2015) argued that initiation of successive MJO events is achieved through the circumnavigation of a fast-moving, dry Kelvin wave from the previous cycle of the MJO. However, numerous modelling results which explicitly removed this pathway for initiation still saw development of successive MJO events (Ray and Li, 2013; Zhao et al., 2013; Maloney and Wolding, 2015). Circumnavigating disturbances could still interfere constructively with the initiating phase of the MJO to promote growth (Maloney and Wolding, 2015), but these modelling studies suggest that the excitation of an MJO event can be caused by the previous event. Heuristically, such an initiation mechanism seems consistent with the notion of absolute instability; the presence of a pulse at some longitude implies the maintenance of the wave amplitude at that position for future times.

The presence or absence of absolute instability is also intricately linked to the group velocity of an unstable wave. Indeed, the presence of absolute instability allows energy to disperse in a direction opposite to the group velocity as evaluated at the most unstable wavenumber. This point is illustrated by Figure 5a; while the group velocity of the peak is obviously eastward, the absolute instability causes wave energy to be dispersed westward as well as eastward. There has been much discussion as to whether the MJO has a westward group velocity, with some observational studies affirming this viewpoint (Adames and Kim, 2016), and others arguing that the group velocity is approximately zero (Chen and Wang, 2018). More recent syntheses of observations have pointed to a diverse range of dispersive behaviours for the MJO (Wei et al., 2023), encompassing both of these previous pictures. Such conclusions are made by tracking the position of successive maxima and minima in precipitation or outgoing longwave radiation through individual or composite MJO events (Adames and Kim, 2016). In this sense, these studies measure the group velocity evaluated at the most unstable wavenumber. From the viewpoint of absolute instability, the more important question is whether the group velocity changes sign within the envelope of the MJO.

A final implication for the intraseasonal variability of the tropics comes from the definition of the WKB solution itself. If we think of the MJO as a local instability of the WP, then its growth rate in time at any point is set not by the local conditions, but instead by conditions at the point at which the absolute growth rate achieves a maximum (Pierrehumbert, 1984). Non-local interactions are a key facet of tropical dynamics, as gravity waves can communicate the effects of convective heating far beyond its actual spatial extent (Gill, 1980; Bretherton and Smolarkiewicz, 1989). Local instability provides another example of the non-local behaviour of the tropics.

## 4.2 | Inclusion of Momentum Damping

The model used in this work was free from any damping in the momentum equation, following previous works on the linear modes of the tropical atmosphere (Adames et al., 2019; Ahmed et al., 2021). However, momentum damping has elsewhere been argued for as an essential component to the dynamics of the MJO (Kim and Zhang, 2021). Zonal momentum budgets suggest that advective tendencies can contribute to a strong effective linear damping rate for the MJO, with a timescale of 3-5 days (Lin et al., 2005). With the inclusion of momentum damping the zonal momentum equation for our system can be rewritten as

$$\frac{\partial u_1}{\partial t} + \frac{\partial \phi_1}{\partial x} = -\varepsilon_u u_1, \tag{20}$$

where $\varepsilon_u$ is a linear damping coefficient that takes on the value of $(3.5 \text{ days})^{-1}$ suggested by Kim and Zhang (2021). The new dispersion relation for the damped system is given by

$$\mathcal{D}(k,\sigma) = i\sigma^2 - \left(c^2k^2\tau_c + \varepsilon_u\right)\sigma - ic^2k^2\left(\tilde{M}_e + i\tilde{A}_q k^{-1}\right) = 0. \tag{21}$$

This system is again quadratic in both $\sigma$ and $k$, so the same analysis methods used in the inviscid system can be applied in a straightforward manner. For real $k$, this modification of the dispersion relation reduces the maximum growth rate of the QE regime, and slows the phase speed slightly (not shown). Figure 12 shows contours of $\sigma$ mapped into the complex $k$-plane under the dispersion relation for the damped system, similar to the mappings shown in Figure 3 for the inviscid system. A merge of the two branches is still evident for the damped system. This merge again appears at intraseasonal time scales, though the absolute growth rate is reduced significantly relative to the undamped system. That absolute instability is still supported with this much reduced growth rate lends us confidence that absolute instability is q quite robust feature of the system when $\tilde{M}_e$ is sufficiently small and $\tau_c$ sufficiently large.

## 4.3 | Caveats

There are a number of caveats to the analysis that we have presented here. Foremost among these concerns is our use of a linear, analytic model to represent the tropical atmosphere and its wave variability. While this choice is made so that we can appeal to the mathematical results provided by Briggs (1964) and Pierrehumbert (1984), in doing so we have neglected much of the complexity of the real MJO. Precipitation is by definition a positive semi-definite quantity. In our linear framework we have implicitly described precipitation as a perturbation upon a precipitating mean state; in general the linear solution will eventually reach an amplitude exceeding this mean state value, and the model becomes physically unreasonable. We have intentionally run our numerical simulations for long times to allow the asymptotic behaviour to dominate, ignoring this deficiency of the linear framework. In reality, there must exist some non-linear process that curtails the linear growth of the wave solutions we have modeled here. Without a strong understanding

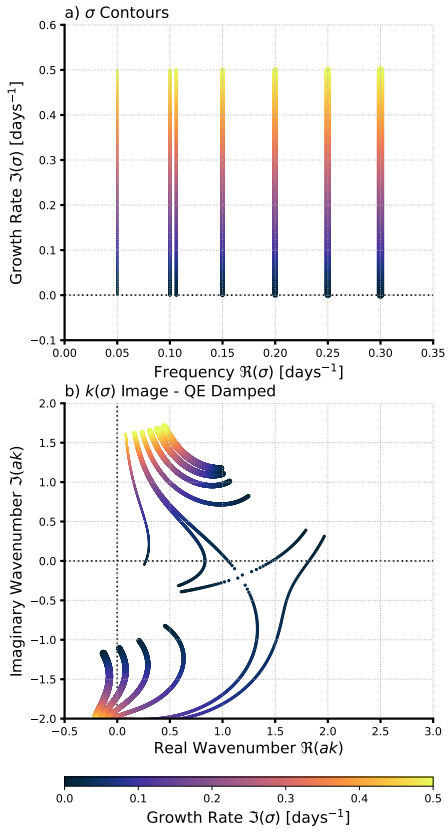


**FIGURE 12** (a) Contours in the $\sigma$-plane which will be mapped into the $k$-plane using the damped dispersion relation. (b) Image of $k(\sigma)$ in the complex $k$-plane for the damped system. An merge between the two branches is located near the real line at $k_r \approx 1.2$, indicating the presence of absolute instability.

of this occlusion process, the actual relevance of the asymptotic limit of the linear system remains uncertain. Rupp and Haynes (2020) show promising results that even in a fully non-linear system, the distinction between absolute and convective instability can influence the dynamics.

Even accepting the necessity of a linear framework to acquire analytical results for unstable waves, our choice of model is not definitive. Each study of the linear modes of tropical variability has its own interpretation of the physical processes needed to represent low-frequency variability (Zhang et al., 2020; Jiang et al., 2020; Fuchs-Stone and Emanuel, 2022). There is considerable uncertainty in the interpretation of the moistening process $\tilde{A_q}$. In our interpretation this parameter is a conglomeration of various terms in the moisture equation, some of which cannot otherwise be easily fit into the first baroclinic mode paradigm with which we work (Sobel and Maloney, 2013; Adames et al., 2019). Analysis of the moisture budget in models or reanalyses can aid in interpretation (Maloney, 2009), but forming a robust connection between the moisture budget and a single linear feedback on the zonal wind will always be challenging. Furthermore, we have represented the effective reduction of the GMS through a cloud-radiation feedback, but modelling results suggest that such a strong feedback may not be necessary to produce MJO variability in the presence of zonal asymmetry (MacDonald and Ming, 2022). This indicates that the parameter $\tilde{M_e}$ should also

be viewed more generally.

Our choice to model intraseasonal variability as a wave with no meridional wind can also be relaxed. The $v = 0$ approximation provides the simplest model for intraseasonal variability, and obviates the need to solve for a complete set of eigenfunctions for the meridional structure. For the exploratory analysis we have performed here, the approximation seems appropriate, in the sense that it captures some of the basic dispersive features of the MJO. The methods used here can be readily applied to systems with more complex meridional structure, either in the long-wave approximation (Heckley and Gill, 1984) or for the full linearized primitive equations on the equatorial $\beta$-plane. Such extensions to the system we have studied have already been derived elsewhere (Fuchs and Raymond, 2017; Ahmed, 2021; Wang and Sobel, 2022b); it would be a valuable exercise to see whether the asymptotic results found here have natural extensions in these systems.

## 5 | CONCLUSIONS

The scale selection and instability of the MJO are often explained via the derivation of linear models that produce a most unstable (real) wavenumber at planetary scales and intraseasonal frequencies. We have instead investigated the asymptotic behaviour of localized pulses, effectively moving away from the normal mode picture that has been focused on in past work. The basis for this analysis is rooted in the theory of absolute and convective instability laid out by Briggs (1964). Using methods described by Briggs (1964) and Pierrehumbert (1986), it was found that simple linear models of the MJO have the property of absolute instability, so that wave amplitude will be seen to grow in a stationary frame of reference. This absolute instability was realized at planetary scales and intraseasonal frequencies, suggesting a potential connection to the MJO. The degree to which the waves were absolutely unstable was shown to be sensitive to certain model parameters. Absolute instability was found to be robust for what we referred to as the quasi-equilibrium (QE) mode, while regimes which produce unstable Kelvin waves were instead only marginally absolutely unstable. Numerical simulations of the model confirmed the predictions made based on the dispersion relation of the system.

The absolute instability of the QE mode was then leveraged to study these linear wave models in a zonally varying flow. Pierrehumbert (1984) stressed that it is in non-uniform systems where the implications of absolute instability become important. We showed that zonal variations which mimic — in an idealized sense — an isolated warm pool can support localized modes of instability through the branch switching inherent to absolute instabilities. A WKB analysis of the system predicted a very asymmetric response across the warm pool. The western flank of the warm pool ($x < 0$) was characterized by temperature and moisture perturbations being in phase, with moisture having a larger magnitude. The eastern part ($x > 0$), on the other hand, featured a quadrature relation between temperature and moisture, with temperature now being greater in magnitude. These predictions were borne out in numerical simulations, which showed strong agreement with the theoretical picture, even when the parameters of the model varied over relatively short length scales.

The proposed significance of these results is that the zonal development of this simple linear model shows some similarity to the way that the MJO develops in its passage across the Indo-Pacific warm pool. We can then think of the essential convection-circulation coupling which gives rise to the temporal instability of the MJO as putting constraints on the nature of spatial instability in the form of amplifying waves. In this sense, our analysis says that low-frequency amplifying waves must have their moist enthalpy more controlled by moisture, and evanescent waves must be controlled by temperature. More work is needed to gain a more physically intuitive picture of why this should be the case. That even this simple model of the MJO can predict this development lends some additional confidence

that it captures some of the essential dynamics of the MJO, and furthers its role as a useful theoretical tool.

Further work is needed to fully understand the implications of absolute instability on moisture-coupled equatorial waves. In particular, uncertainties related to the occlusion of linear growth by non-linear processes mean that conclusions based on the asymptotic behaviour of the system must be viewed with caution. This work joins a selection of previous works (Diaz and Aiyyer, 2015; Rupp and Haynes, 2020) which suggest that a greater understanding of atmospheric waves can be attained through the consideration of their spatial instability. Further extension of these concepts to the off-equator moisture waves of Sobel et al. (2001) and Adames and Ming (2018) would be an interesting venture. This initial investigation provides evidence for the relevance of absolute instability to our understanding of the MJO and convectively-coupled equatorial waves. In doing so, it provides a new perspective on tropical dynamics and drives home the critical role of zonal asymmetry in setting the behaviour of these waves.

## Acknowledgements

I would like to thank Isaac Held for introducing me to the concepts of absolute and convective instability, and for helpful comments during the writing of this manuscript. Further comments from Yi Ming and Wanying Kang were much appreciated. This research was supported by the Co-operative Institute for Modeling the Earth System (CIMES) at Princeton University and NOAA GFDL.

## Data Availability Statement

The analysis and plots that were generated for this work are accessible in the form of Jupyter Notebooks at https://doi.org/10.5281/zenodo.7908479

## references

Adames, Á. F. and Kim, D. (2016) The mjo as a dispersive, convectively coupled moisture wave: Theory and observations. *Journal of the Atmospheric Sciences*, **73**, 913–941.

Adames, Á. F., Kim, D., Clark, S. K., Ming, Y. and Inoue, K. (2019) Scale analysis of moist thermodynamics in a simple model and the relationship between moisture modes and gravity waves. *Journal of the Atmospheric Sciences*, **76**, 3863–3881.

Adames, A. F. and Maloney, E. D. (2021) Moisture mode theory's contribution to advances in our understanding of the madden-julian oscillation and other tropical disturbances. *Current Climate Change Reports*, **7**, 72–85.

Adames, Á. F. and Ming, Y. (2018) Interactions between water vapor and potential vorticity in synoptic-scale monsoonal disturbances: Moisture vortex instability. *Journal of the Atmospheric Sciences*, **75**, 2083–2106.

Ahmed, F. (2021) The mjo on the equatorial beta plane: An eastward-propagating rossby wave induced by meridional moisture advection. *Journal of the Atmospheric Sciences*, **78**, 3115–3135.

Ahmed, F., Neelin, J. D. and Adames, Á. F. (2021) Quasi-equilibrium and weak temperature gradient balances in an equatorial beta-plane model. *Journal of the Atmospheric Sciences*, **78**, 209–227.

Bretherton, C. S. and Smolarkiewicz, P. K. (1989) Gravity waves, compensating subsidence and detrainment around cumulus clouds. *Journal of Atmospheric Sciences*, **46**, 740–759.

Briggs, R. J. (1964) *Electron-stream interaction with plasmas*, vol. 187. MIT press Cambridge, MA.

Chen, G. and Wang, B. (2018) Does the mjo have a westward group velocity? *Journal of Climate*, **31**, 2435–2443.

Diaz, M. and Aiyyer, A. (2015) Absolute and convective instability of the african easterly jet. *Journal of the Atmospheric Sciences*, **72**, 1805–1826.

Durran, D. R. (2013) *Numerical methods for wave equations in geophysical fluid dynamics*, vol. 32. Springer Science & Business Media.

Emanuel, K. A., David Neelin, J. and Bretherton, C. S. (1994) On large-scale circulations in convecting atmospheres. *Quarterly Journal of the Royal Meteorological Society*, **120**, 1111–1143.

Farrell, B. F. (1982) Pulse asymptotics of the charney baroclinic instability problem. *Journal of Atmospheric Sciences*, **39**, 507–517.

Fuchs, Ž. and Raymond, D. J. (2017) A simple model of intraseasonal oscillations. *Journal of Advances in Modeling Earth Systems*, **9**, 1195–1211.

Fuchs-Stone, Ž. and Emanuel, K. (2022) Sensitivity of linear models of the madden–julian oscillation to convective representation. *Journal of the Atmospheric Sciences*, **79**, 1575–1584.

Fulton, S. R. and Schubert, W. H. (1985) Vertical normal mode transforms: Theory and application. *Monthly weather review*, **113**, 647–658.

Gaster, M. (1968) Growth of disturbances in both space and time. *The Physics of Fluids*, **11**, 723–727.

Gill, A. E. (1980) Some simple solutions for heat-induced tropical circulation. *Quarterly Journal of the Royal Meteorological Society*, **106**, 447–462.

Heckley, W. and Gill, A. (1984) Some simple analytical solutions to the problem of forced equatorial long waves. *Quarterly Journal of the Royal Meteorological Society*, **110**, 203–217.

Hendon, H. H. and Salby, M. L. (1994) The life cycle of the madden–julian oscillation. *Journal of Atmospheric Sciences*, **51**, 2225–2237.

Huerre, P. and Monkewitz, P. A. (1985) Absolute and convective instabilities in free shear layers. *Journal of Fluid Mechanics*, **159**, 151–168.

— (1990) Local and global instabilities in spatially developing flows. *Annual review of fluid mechanics*, **22**, 473–537.

Inoue, K. and Back, L. E. (2017) Gross moist stability analysis: Assessment of satellite-based products in the gms plane. *Journal of the Atmospheric Sciences*, **74**, 1819–1837.

Inoue, K., Biasutti, M. and Fridlind, A. M. (2021) Evidence that horizontal moisture advection regulates the ubiquitous amplification of rainfall variability over tropical oceans. *Journal of the Atmospheric Sciences*, **78**, 529–547.

Jiang, X., Adames, Á. F., Kim, D., Maloney, E. D., Lin, H., Kim, H., Zhang, C., DeMott, C. A. and Klingaman, N. P. (2020) Fifty years of research on the madden-julian oscillation: Recent progress, challenges, and perspectives. *Journal of Geophysical Research: Atmospheres*, **125**, e2019JD030911.

Kiladis, G. N., Wheeler, M. C., Haertel, P. T., Straub, K. H. and Roundy, P. E. (2009) Convectively coupled equatorial waves. *Reviews of Geophysics*, **47**.

Kim, J.-E. and Zhang, C. (2021) Core dynamics of the mjo. *Journal of the Atmospheric Sciences*, **78**, 229–248.

Lin, J.-L., Zhang, M. and Mapes, B. (2005) Zonal momentum budget of the madden–julian oscillation: The source and strength of equivalent linear damping. *Journal of the atmospheric sciences*, **62**, 2172–2188.

Lin, S. and Pierrehumbert, R. T. (1993) Is the midlatitude zonal flow absolutely unstable? *Journal of Atmospheric Sciences*, **50**, 505–517.

MacDonald, C. G. and Ming, Y. (2022) Tropical intraseasonal variability response to zonally asymmetric forcing in an idealized moist gcm. *Journal of Climate*, **35**, 4479–4501.

Majda, A. J. and Stechmann, S. N. (2011) Nonlinear dynamics and regional variations in the mjo skeleton. *Journal of the Atmospheric Sciences*, **68**, 3053–3071.

Maloney, E. D. (2009) The moist static energy budget of a composite tropical intraseasonal oscillation in a climate model. *Journal of Climate*, **22**, 711–729.

Maloney, E. D., Sobel, A. H. and Hannah, W. M. (2010) Intraseasonal variability in an aquaplanet general circulation model. *Journal of Advances in Modeling Earth Systems*, **2**.

Maloney, E. D. and Wolding, B. O. (2015) Initiation of an intraseasonal oscillation in an aquaplanet general circulation model. *Journal of Advances in Modeling Earth Systems*, **7**, 1956–1976.

Matthews, A. J. (2008) Primary and successive events in the madden–julian oscillation. *Quarterly Journal of the Royal Meteorological Society: A journal of the atmospheric sciences, applied meteorology and physical oceanography*, **134**, 439–453.

Mayta, V. C. and Adames, Á. F. (2023) Moist thermodynamics of convectively coupled waves over the western hemisphere. *Journal of Climate*, 1–35.

Merkine, L.-O. (1977) Convective and absolute instability of baroclinic eddies. *Geophysical & Astrophysical Fluid Dynamics*, **9**, 129–157.

Merkine, L.-O. and Shafranek, M. (1980) The spatial and temporal evolution of localized unstable baroclinic disturbances. *Geophysical & Astrophysical Fluid Dynamics*, **16**, 175–206.

Neelin, J. D. and Yu, J.-Y. (1994) Modes of tropical variability under convective adjustment and the madden–julian oscillation. part i: Analytical theory. *Journal of Atmospheric Sciences*, **51**, 1876–1894.

Pierrehumbert, R. (1984) Local and global baroclinic instability of zonally varying flow. *Journal of Atmospheric Sciences*, **41**, 2141–2162.

Pierrehumbert, R. T. (1986) Spatially amplifying modes of the charney baroclinic-instability problem. *Journal of Fluid Mechanics*, **170**, 293–317.

Powell, S. W. and Houze Jr, R. A. (2015) Effect of dry large-scale vertical motions on initial mjo convective onset. *Journal of Geophysical Research: Atmospheres*, **120**, 4783–4805.

Ray, P. and Li, T. (2013) Relative roles of circumnavigating waves and extratropics on the mjo and its relationship with the mean state. *Journal of the atmospheric sciences*, **70**, 876–893.

Raymond, D. J. and Fuchs, Ž. (2018) The madden-julian oscillation and the indo-pacific warm pool. *Journal of Advances in Modeling Earth Systems*, **10**, 951–960.

Roundy, P. E. (2012) The spectrum of convectively coupled kelvin waves and the madden–julian oscillation in regions of low-level easterly and westerly background flow. *Journal of the atmospheric sciences*, **69**, 2107–2111.

Rupp, P. M. and Haynes, P. H. (2020) Spatio-temporal stability analysis applied to monsoon anticyclone flow. *Quarterly Journal of the Royal Meteorological Society*, **146**, 1861–1879.

Simmons, A. J. and Hoskins, B. J. (1979) The downstream and upstream development of unstable baroclinic waves. *Journal of the Atmospheric Sciences*, **36**, 1239–1254.

Sobel, A. and Kim, D. (2012) The mjo-kelvin wave transition. *Geophysical research letters*, **39**.

Sobel, A. and Maloney, E. (2013) Moisture modes and the eastward propagation of the mjo. *Journal of the Atmospheric Sciences*, **70**, 187–192.

Sobel, A. H., Nilsson, J. and Polvani, L. M. (2001) The weak temperature gradient approximation and balanced tropical moisture waves. *Journal of the atmospheric sciences*, **58**, 3650–3665.

Wang, S. and Sobel, A. H. (2022a) A filtered model for the tropical intraseasonal moisture mode. *Geophysical Research Letters*, **49**, e2022GL098320.

— (2022b) A unified moisture mode theory for the madden–julian oscillation and the boreal summer intraseasonal oscillation. *Journal of Climate*, **35**, 1267–1291.

Wei, Y., Ren, H.-L., Xiang, B., Wang, Y., Wu, J. and Wang, S. (2023) Diverse mjo genesis and predictability. *Bulletin of the American Meteorological Society*, **104**, E792–E809.

Zhang, C., Adames, Á., Khouider, B., Wang, B. and Yang, D. (2020) Four theories of the madden-julian oscillation. *Reviews of Geophysics*, **58**, e2019RG000685.

Zhao, C., Li, T. and Zhou, T. (2013) Precursor signals and processes associated with mjo initiation over the tropical indian ocean. *Journal of Climate*, **26**, 291–307.